

Inhibition of the corrosion of mild steel in acidic media by use of a new antipyridine derivative

P. Muthukrishnan · B. Jeyaprabha · P. Tharmaraj · P. Prakash

Received: 16 January 2014 / Accepted: 12 May 2014 / Published online: 7 June 2014
© Springer Science+Business Media Dordrecht 2014

Abstract The activity of 4-[5-((4-chlorophenyl)diazenyl)-2-hydroxybenzylideneamino)-1,5-dimethyl-2-phenyl-1*H*-pyrazole-3-(2*H*)-one (CDHBAP) against corrosion of mild steel in 1 M H₂SO₄ solutions has been investigated by measurement of weight loss and by potentiodynamic polarization and AC impedance studies. The results obtained indicate that CDHBAP is a good inhibitor; its efficiency reaches 99 % at 100 ppm. Polarization studies show that CDHBAP inhibits corrosion of mild steel by means of a mixed-mode mechanism. AC impedance results confirm adsorption of the CDHBAP at the mild steel–acid interface. A decrease in inhibition efficiency is observed with increasing temperature, and activation energies increase in the presence of CDHBAP. Physical adsorption is proposed from the trend of inhibition efficiency and the values of ΔG_{ads}^0 . Formation of a protective layer against acid attack was confirmed by use of FT-IR and UV–visible spectroscopy, X-ray diffraction analysis, and scanning electron microscopy.

Keywords Mild steel · Electrochemical techniques · FT-IR · XRD · Acid corrosion

Introduction

Acids, for example hydrochloric acid and sulfuric acid, are commonly used as industrial pickling, descaling, and cleaning agents for removal of undesirable oxide

P. Muthukrishnan · P. Tharmaraj · P. Prakash (✉)
Department of Chemistry, Thiagarajar College, Madurai 625009, India
e-mail: kmpprakash@gmail.com

B. Jeyaprabha
Department of Civil Engineering, Fatima Michael College of Engineering & Technology,
Madurai 625 020, India

film and corrosion products [1–5]. In many industries, mild steel is a common construction material in the fabrication of reaction vessels, pipelines in the petroleum industry, machinery, storage tanks, and chemical batteries, etc., which corrode easily in the presence of acids. Inhibitors are used in acid solutions to minimize the corrosion of mild steel during the acid cleaning and descaling. Literature survey revealed that many organic compounds have been studied to evaluate their effectiveness as inhibitors of acid corrosion [6–9]. Heterocyclic compounds, for example pyrazole, triazole, tetrazole, benzotriazole, benzimidazole, and benzothiazole derivatives, have been reported to very good inhibitors for mild steel in different media [10–17]. Among the different nitrogen and sulfur compounds studied as inhibitors, pyrazoles are regarded as environmentally acceptable chemicals. Many substituted pyrazole compounds have recently been studied in considerable detail as effective corrosion inhibitors for mild steel in acidic media [18–24]. Inhibition by these organic compounds is usually attributed to their interaction with the mild steel surface via adsorption. Adsorption of an inhibitor by a metal surface depends on the nature and surface charge on the metal, the mode of adsorption, the chemical structure of the inhibitor, and the type of electrolyte solution.

The objective of this work was to study the inhibitive effect of CDHBAP on corrosion of mild steel in 1 M H₂SO₄ solution. Inhibition of corrosion by CDHBAP was studied by measurement of weight loss, investigation of the effect of temperature, study of potentiodynamic polarization, use of AC impedance spectroscopy, UV–visible and FT-IR spectroscopy, X-ray diffraction (XRD) analysis, and scanning electron microscopy (SEM). Thermodynamic and kinetic data were also evaluated.

Experimental

Preparation of materials

Mild steel specimens of weight percentage composition C 0.05 %, Mn 0.6 %, P 0.36 %, Si 0.03 %, and the balance Fe were mechanically cut into 2.5 cm × 2.5 cm × 0.4 cm pieces for study of weight loss and the effect of temperature. Mild steel specimens of the same composition embedded in Araldite, with an exposed area of 0.5 cm², were used as electrodes for electrochemical measurements. The electrodes were polished by use of a sequence of different emery papers up to 4/0 grade, then washed with acetone, dried at room temperature, and stored in a moisture-free desiccator until used for corrosion tests. Acid solutions (1 M H₂SO₄) were prepared in triple-distilled water from AR grade H₂SO₄.

Synthesis of CDHBAP

The diazonium salt 5-((4-chlorophenyl)diazonyl)-2-hydroxybenzaldehyde (CPDAHP) (2.60 g, 10 mmol) in ethanol was condensed by heating under reflux in an ethanolic solution of 1-phenyl-2,3-dimethyl-4-aminopyrazol-5-one (4-AAP) (2.03 g, 10 mmol)

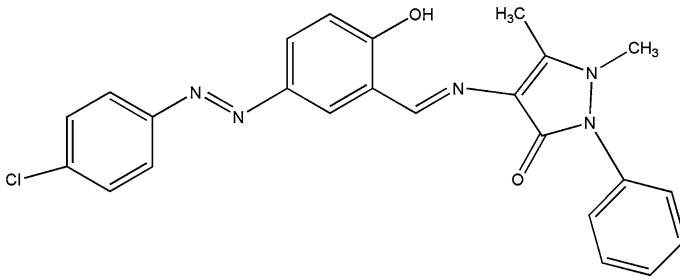


Fig. 1 Molecular structure of CDHBAP

for 3 h. The solution was left to stand at room temperature and the solid obtained was washed with ethanol and recrystallized [25]. The molecular structure of CDHBAP is given in Fig. 1.

Weight-loss measurements

Measurement of weight-loss is the easiest method of determination of the rate of corrosion and of inhibition efficiency. In our study, mild steel specimens were immersed in 1 M H_2SO_4 solution (100 mL) without and with the inhibitor at different concentrations and at different temperatures (308–328 K) for 2 h. After immersion for 2 h, the specimens were removed from the solution, rinsed with double-distilled water, washed with acetone, dried thoroughly, and weighed. The mass of the mild steel specimens before and after immersion was determined by use of an analytical balance with precision of 0.1 mg. Experiments were performed in triplicate and mass losses were averaged. The weight loss (ΔW) was used to calculate the rate of corrosion (CR) and the efficiency of inhibition (IE, %):

$$\text{CR(mpy)} = 534 \times (W_b - W_a) / DST \quad (1)$$

$$\text{IE \%} = (W_0 - W_i) / W_0 \times 100 \quad (2)$$

where W_b and W_a are the weights of the specimen before and after immersion in the solutions tested, W_0 and W_i are the weight loss (g) of mild steel in the absence and presence of CDHBAP respectively, D is the density of mild steel (7.8 g cm^{-3}), S is the area of the specimen (cm^2), and T is the period of immersion (h).

Electrochemical measurements

Potentiodynamic polarization measurements

A CH electrochemical analyzer, model 604D, was used to record Tafel polarization curves. A three-electrode cell assembly was used. The working electrode (0.5 cm^2 mild steel) was exposed to the acid solutions in the absence and presence of CDHBAP. Platinum and saturated calomel electrodes (SCE) were used as counter electrode and reference electrode, respectively. All electrochemical measurements

were conducted at 308 K using 100 mL electrolyte (1 M H₂SO₄) under stationary conditions. Before potentiodynamic polarization (Tafel) and electrochemical impedance spectroscopy (EIS) measurement, the electrode was immersed in test solution at open circuit potential (OCP) for 30 min to achieve a stable state. Potentiodynamic polarization curves were recorded from -300 to $+300$ mV_{SCE} (versus OCP) at a scan rate of 1 mV/s. All the potentials reported were with reference to SCE.

AC impedance measurement

This study was conducted with a CH electrochemical analyzer, model 604D. The cell was the same as that used for polarization measurements. AC impedance measurements were performed in the frequency range 0.1 Hz–100 kHz with a peak-to-peak amplitude of 5 mV. The real part and imaginary parts of the cell impedance were measured in ohms for different frequencies. The charge-transfer resistance (R_{ct}) and double-layer capacitance (C_{dl}) were calculated by use of the relationships:

$$R_{ct} = (R_s + R_{ct}) - R_s \quad (3)$$

$$C_{dl} = 1/2\pi R_{ct} f_{max} \quad (4)$$

where f_{max} is the frequency at the maximum of the Nyquist plot and R_s is the solution resistance. Each experiment was run in triplicate to check the reproducibility of the data.

Spectral and surface morphology studies

Fourier transform-infrared spectroscopy (FT-IR)

FT-IR spectra were recorded by use of a Shimadzu FTIR-8400S spectrophotometer. The spectra of CDHBAP and the protective film formed on the mild steel surface were recorded by carefully removing the film, mixing with a small amount of KBr powder, and preparation of a disk.

Ultraviolet spectroscopy

UV–visible absorption spectrophotometry was performed on the prepared mild steel specimens after immersion in acid solution (1 M H₂SO₄) with the optimum concentration of inhibitor (100 ppm) at 308 K for 2 h. UV–visible spectra of pure CDHBAP were also obtained. UV–visible absorption spectra were acquired by use of a Jasco V 530 spectrophotometer.

X-ray diffraction and SEM characterization

The mild steel specimens were immersed in the 1 M H₂SO₄ solutions in the absence and presence of the optimum concentration of corrosion inhibitor for a period of 2 h. After 2 h the specimens were removed and dried. The nature of the film formed

on the surface of mild steel specimens was examined by use of an XRD goniometer (Shimadzu model XRD 6000) and a scanning electron microscope (Jeol JSM 6390).

Results and discussion

Effect of inhibitor concentration

The efficiency of inhibition (%) and rate of corrosion (CR) obtained from measurement of weight loss for different concentrations of CDHBAP at 308–328 K are summarized in Table 1. From this table it is clear that percentage inhibition increases with increasing concentration of CDHBAP. This indicates that surface coverage of metal by adsorption of CDHBAP increases with increasing concentration of CDHBAP. Maximum efficiency of inhibition by the compound (94.26 % in H_2SO_4) is observed at a concentration of 100 ppm (optimum concentration). A further increase of inhibitor concentration does not significantly change the protective effect. This can be attributed to maximum adsorption of CDHBAP by the mild steel surface. The constant efficiency above 100 ppm can be attributed to competition for adsorption of inhibitor molecules by the metal surface (which in 100-ppm solution is completely coated by molecules) and/or return of adsorbed CDHBAP to the bulk solution [26].

Effect of exposure time

Immersion time is an important condition which can be used to evaluate the stability of inhibitor behavior [27]. Figure 2 shows the variation of weight loss with time for corrosion of mild steel in 1 M H_2SO_4 in the absence and presence of different concentrations of CDHBAP for 2, 6, 12, 18, and 24 h at 308 K. From the figure, it is apparent that weight loss of mild steel increases with increasing contact time. The rate of corrosion decreases with increasing concentration of CDHBAP, which indicates that CDHBAP retards the rate of corrosion of mild steel in 1 M H_2SO_4 solutions. This inhibitor contains oxygen, nitrogen, and an aromatic ring as centers of adsorption. At high temperature (313–328 K; plots not shown), weight loss of mild steel is found to increase with increasing temperature, indicative of desorption of the adsorbed protective film at high temperatures [28, 29].

Effect of temperature

Temperature is an important condition in studies of metal dissolution. The effect of temperature on the inhibited acid–metal reaction is very complex because, many changes may occur on the metal surface, for example rapid etching, desorption of inhibitor, and decomposition of the inhibitor. The inhibition properties of CDHBAP can also be explained on the basis of a kinetic model. Thermodynamic activation data for the corrosion process were calculated by use of the Arrhenius equation (Eq. 5) and the transition equation (Eq. 6) [30]:

Table 1 Rate of corrosion and efficiency of inhibition results obtained from measurement of weight loss in 1 M H₂SO₄ solution in the absence and presence of CDHBAP at different temperatures

Concentration of CDHBAP (ppm)	Rate of corrosion (mpy)					Inhibition efficiency (%)				
	308 K	313 K	318 K	323 K	328 K	308 K	313 K	318 K	323 K	328 K
0	3.2846	5.0552	7.2108	8.6286	9.2094	–	–	–	–	–
15	0.4299	0.7626	1.6154	2.7407	3.4675	86.91	84.91	77.59	68.23	62.34
25	0.3707	0.6340	1.3326	2.4893	2.9681	88.71	87.45	81.51	71.14	67.77
35	0.2904	0.4852	1.0405	2.1164	2.7010	91.15	90.40	85.56	75.47	70.67
70	0.2030	0.3794	0.8641	1.6159	2.4725	93.81	92.49	88.01	81.27	73.15
100	0.1883	0.3028	0.6980	1.5008	2.0203	94.26	94.00	90.31	82.60	78.06

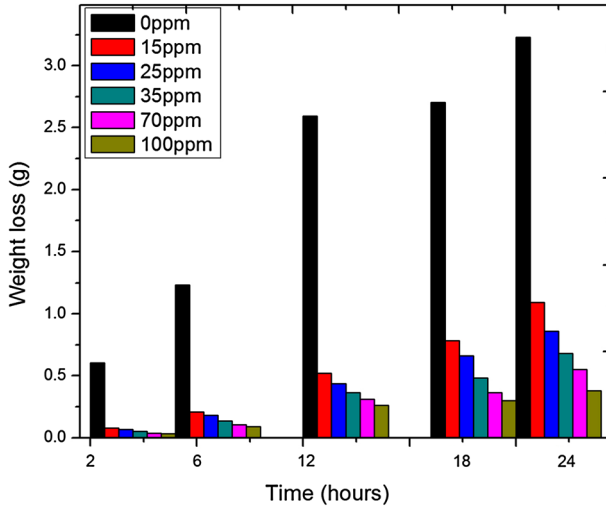


Fig. 2 Variation of weight loss with exposure time for corrosion of mild steel in 1 M H₂SO₄

$$\log CR = \log A - (E_a/2.303RT) \tag{5}$$

$$\log CR/T = \{\log(R/hN) + (\Delta S^*/2.303R)\} - (\Delta H^*/2.303RT) \tag{6}$$

where CR is the rate of corrosion, *A* is the frequency factor, *T* is the temperature, *E_a* is the apparent activation energy, *R* is the molar gas constant, *h* is plank’s constant, *N* is Avogadro’s number, ΔS is the entropy of activation, and ΔH is the enthalpy of activation.

The Arrhenius plot of log CR versus 1/*T* for corrosion of mild steel in 1 M H₂SO₄ solution in the absence and presence of different concentrations of CDHBAP is shown in Fig. 3.

The values of apparent activation energy (*E_a*) obtained from the slope, $-E_a/2.303R$, of the lines and the pre-exponential factors, *A*, obtained from the intercept, log *A*, are given in Table 2. Values of *E_a* ranged from 43.85 to 106.7 kJ/mol for inhibited H₂SO₄ solution. In this study the apparent activation energy (*E_a*) increased with increasing CDHBAP concentration, and was higher than that in the absence of inhibitor (Table 2). This clearly indicates that adsorption of the inhibitor by the metal surface decreases with increasing temperature [31]. Relationships between the temperature dependence of efficiency of inhibition and *E_a* can be classified into three groups, depending to the effect of temperature [32]:

- 1 if IE decreases with increasing temperature, *E_a* (inhibited solution) > *E_a* (uninhibited solution);
- 2 if IE increases with increasing temperature, *E_a* (inhibited solution) < *E_a* (uninhibited solution); and
- 3 if IE does not change with temperature, *E_a* (inhibited solution) = *E_a* (uninhibited solution).

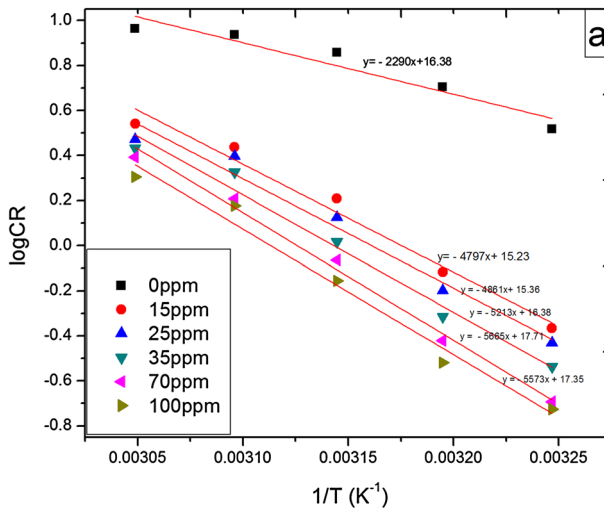


Fig. 3 Arrhenius plots of log CR versus $1/T$ for mild steel in 1 M H_2SO_4 and in the presence of different concentrations of CDHBAP

Table 2 Activation data for mild steel in 1 M H_2SO_4 solution in the absence and presence of different concentrations of CDHBAP

Concentration of CDHBAP (ppm)	E_a (kJ/mol)	A	ΔH^* (kJ/mol)	ΔS^* (J/K/mol)
0	43.85	1.00×10^8	41.20	-100.59
15	91.85	1.69×10^{15}	89.21	37.74
25	93.07	2.29×10^{15}	90.43	40.42
35	99.81	2.39×10^{16}	97.17	59.95
70	108.46	5.12×10^{17}	105.82	85.23
100	106.70	2.13×10^{17}	104.06	78.34

In this investigation, the inhibitor falls into group 1, because E_a (inhibited solution) $>$ E_a (uninhibited solution) and E_a increases with increasing inhibitor concentration, which further confirms that IE (%) decreases with increasing temperature.

Figure 4 shows the plot of log CR/T against $1/T$. Straight lines were obtained with a slope of $\Delta H^*/2.303R$ and an intercept of $\log(R/Nh) + (\Delta S^*/2.303R)$, from which the values of ΔS^* and ΔH^* were calculated; these are included in Table 2. In this system, the positive sign of enthalpies reflects the endothermic nature of dissolution of steel, implying inferring that dissolution of mild steel is difficult [30, 33]. The shift toward the positive values of the entropy of activation both in the absence and the presence of the inhibitor imply that the activated complex in the rate determining step represents dissociation rather than association, meaning that disordering increases on going from reactants to the activated complex [34–37]. The results are comparable with those obtained for previously reported organic inhibitors [23].

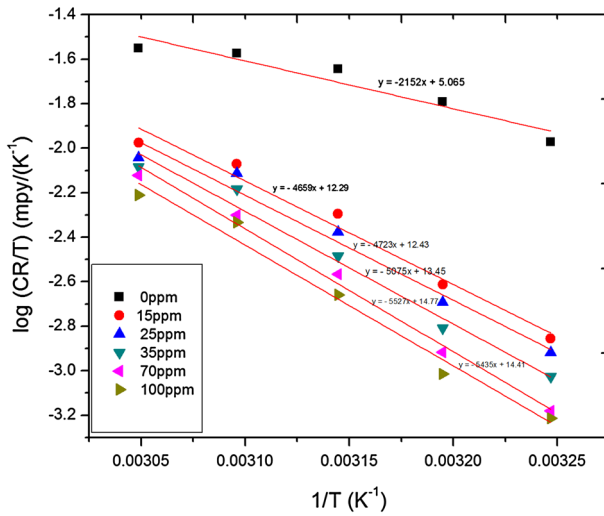


Fig. 4 Transition state plots of log CR/T versus 1/T for mild steel in 1 M H₂SO₄ and in the presence of different concentrations of CDHBAP

Adsorption isotherms

Adsorption isotherms are very important for determining the mechanism of organo–electrochemical reaction. Adsorption is usually regarded as a process of substitution of water molecules adsorbed at the metal–solution interface by the organic molecules of the inhibitor. A correlation between surface coverage (θ) and inhibitor concentration (C) in the electrolyte can be represented by the Langmuir adsorption isotherm:

$$C/\theta = 1/K_{ads} + C \tag{7}$$

where C is the concentration of inhibitor (ppm), K is the adsorption–desorption equilibrium constant, and θ is the surface coverage, which is given by:

$$\theta = \% IE/100. \tag{8}$$

Straight lines were obtained when C/θ was plotted against C (g/l) (Fig. 5). The correlation coefficient (r^2) was used to choose the type of isotherm that was the best fit with the experimental data. These plots suggest that adsorption of inhibitors (CDHBAP) by the metal surface obeys the Langmuir adsorption isotherm. From the intercept of the straight lines, the values of K_{ads} were calculated and are summarized in Table 3.

The standard free energy of adsorption ($-\Delta G_{ads}^0$) and the equilibrium constant (K_{ads}) are related by the equation:

$$\Delta G_{ads}^0 = -RT \ln(55.5 \times K_{ads}) \tag{9}$$

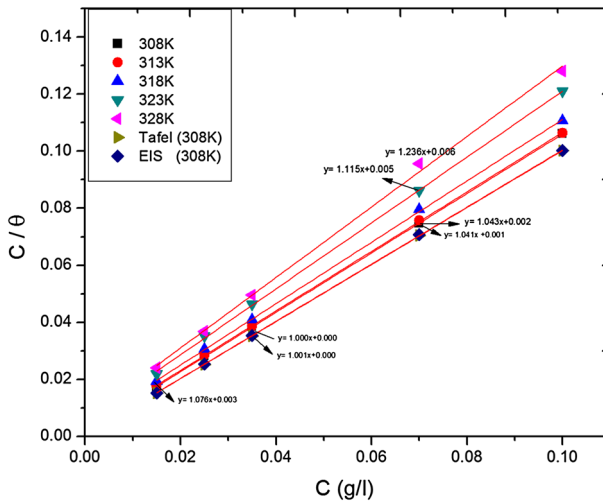


Fig. 5 Langmuir adsorption isotherms for adsorption of CDHBAP on mild steel in 1 M H₂SO₄ solution, obtained by use of Tafel and EIS measurements at 308 K

Table 3 Thermodynamic data for adsorption of CDHBAP on mild steel in 1 M H₂SO₄ at different temperatures

Temperature (K)	$-\Delta G_{\text{ads}}^0$ (kJ/mol)	ΔH_{ads} (kJ/mol)	$-\Delta S_{\text{ads}}$ (J/mol/K)	R^2	K_{ads} (L/mol)
308	12.355		20.60	1.000	2.245
313	10.751		20.78	0.999	1.122
318	9.852	-75.81	20.74	0.999	0.748
323	8.635		20.79	0.999	0.449
328	8.272		20.59	0.998	0.374

where R is the gas constant, T is the temperature, and 55.5 is the molar concentration of water in solution. K_{ads} decreases with increasing temperature, showing that the interactions between the adsorbed molecules and the metal surface are weakened and the inhibitor molecules are easily removed. Such data explain the decrease in the efficiency of protection with increasing temperature. The negative values of ΔG_{ads}^0 clearly indicated that spontaneous adsorption of CDHBAP by the mild steel surface was a physical process. In general, values of ΔG_{ads}^0 up to -20 kJ/mol are consistent with electrostatic interaction between charged molecules and the charged metal, i.e. physical adsorption. Values of approximately -40 kJ/mol or higher are associated with chemisorption, which results from sharing or transfer of unshared electron pairs or π -electrons of organic molecules with the metal surface to form a coordinate type of bond [38, 39]. In this study, calculated values of ΔG_{ads}^0 were < -20 kJ/mol, indicating that physical adsorption of the inhibitor occurred on the metal surface. The enthalpy and entropy of adsorption are important properties for understanding adsorption of organic inhibitors at the metal–solution interface. The enthalpy of adsorption (ΔH_{ads}) is calculated by use of the van't Hoff equation:

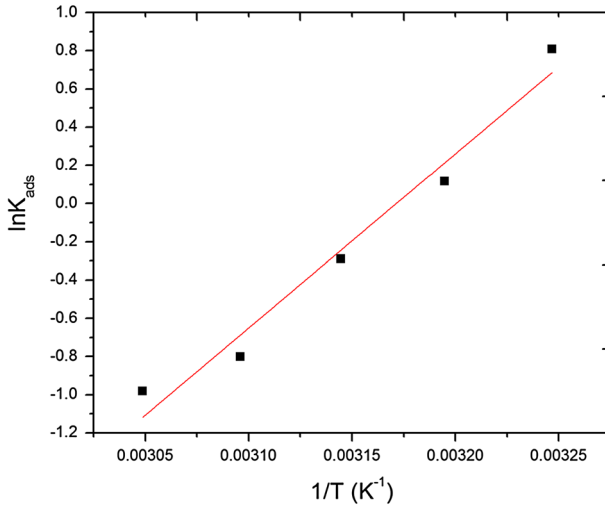


Fig. 6 The relationship between $\ln K_{ads}$ and $1/T$ for CDHBAP on mild steel in acid solutions

$$\ln K_{ads} = -\Delta H_{ads}/RT + \text{constant} \tag{10}$$

Figure 6 shows the straight-line of plot of $\ln K_{ads}$ against $1/T$.

The slope of this line is $-\Delta H_{ads}/R$. The enthalpy of adsorption can be approximately regarded as the standard enthalpy of adsorption (ΔH_{ads}) under these experimental conditions. The standard entropy of adsorption (ΔS_{ads}) is obtained by use of the basic thermodynamic equation:

$$\Delta S_{ads} = \frac{\Delta H_{ads} - \Delta G_{ads}^0}{T} \tag{11}$$

The calculated thermodynamic data are listed in Table 3. Values of ΔH_{ads} were negative, suggesting that adsorption of the inhibitor is an exothermic process, which means that the efficiency of inhibition is lower at high temperature, as a result of gradual desorption of the inhibitor from the mild steel surface [28, 29]. The values of ΔS_{ads} are nearly constant and negative, ranging between -20.79 and -20.59 J/mol/K at temperatures in the range 308–328 K. This behavior is explained as follows. Before adsorption of the inhibitor molecules on the mild steel surface they move freely (chaotically) in the bulk solution whereas on adsorption they become distributed in an orderly fashion on the steel surface; as a result a decrease in entropy is observed [27, 40].

Potentiodynamic polarization measurements

Potentiodynamic polarization measurements were performed to study the kinetics of the cathodic and anodic reactions. Figure 7 shows the polarization curves for mild steel in 1 M H_2SO_4 solution. It is obvious that the cathodic branch has typical Tafel behavior. This makes it possible, as will be seen, to accurately evaluate the cathodic

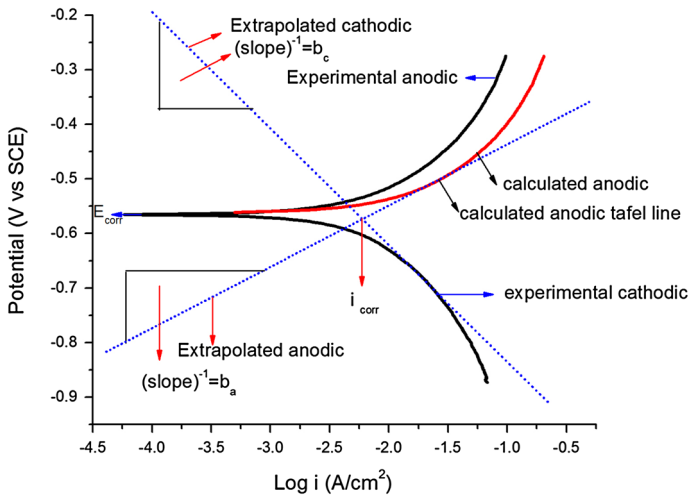


Fig. 7 Anodic and cathodic polarization curves recorded for mild steel in 1 M H₂SO₄ after immersion for 2 h at 308 K

Tafel slope (b_c) and corrosion currents (i_{corr}) by the Tafel extrapolation method. The anodic polarization curve does not have the expected log–linear Tafel behavior over the complete range of potential, however. The curvature of the anodic branch may be attributed to deposition of corrosion products or impurities in the steel to form a non-passive film [41]. Likhanova et al. [42] recently tested some synthesized ionic liquids as inhibitors of corrosion of mild steel in sulfuric acid by use of polarization measurements complemented with surface analysis (SEM, EDX, XRD, and Mossbauer spectroscopy). They reported adsorption of corrosion products with low solubility, for example iron sulfates such as melanterite, rosenite, szomolnokite, etc., and oxyhydroxides such as goethite, which may have effect on the polarization curve.

Therefore, because of the absence of linearity of the anodic branch, accurate evaluation of the anodic Tafel slope by Tafel extrapolation of the anodic branch is impossible [41, 43, 44]. There is, therefore, uncertainty and error in numerical values of the anodic Tafel slope (b_a); there may also be errors in the values of i_{corr} , calculated by use of software. This is why we did not introduce here i_{corr} or b_a values determined by use of software. It has been shown that in use of the Tafel extrapolation method, use of both anodic and cathodic Tafel regions is undoubtedly preferred to use of one Tafel region only.

However, the rate of corrosion can also be determined by Tafel extrapolation of either the cathodic or anodic polarization curve alone. If only one polarization curve is used, it is usually the cathodic curve which produces a longer and better defined Tafel region (as in this work). Anodic polarization may sometimes produce concentration effects, because of passivation and dissolution, as noted above, and roughening of the surface which can lead to deviations from Tafel behavior. Thus extrapolation of the cathodic Tafel region back to zero overvoltage gives the net rate

of the cathodic reaction at the corrosion potential [45]. Consequently, it is possible to calculate the anodic Tafel line from the experimental data shown in Fig. 7. The Tafel line of the cathodic polarization curve is first extended from the linear region of the Tafel line to electrode potentials below the corrosion potential. The anodic current density i_a is calculated from [45]:

$$(i_{\text{net}})_a = [(i_{\text{Fe}})_a + (i_{\text{H}})_a] - [(|i_{\text{Fe}}|)_c + (|i_{\text{H}}|)_c] \tag{12}$$

or, simply:

$$i_a(\text{net experimental}) = i_a - |i_c| \tag{13}$$

where the subscripts “a” and “c” refer to the anodic and cathodic directions, respectively. Thus, $(i_{\text{Fe}})_a$ and $(|i_{\text{H}}|)_c$, refer, respectively, to anodic dissolution of Fe and the cathodic hydrogen evolution reaction. $|i_c|$ is the cathodic current density. Thus, the calculated anodic current density, i_a , is the sum of the experimentally observed anodic current density and the extrapolated cathodic current density. On the basis of these calculations, a corrosion current density (i_{corr}) of 6,025 $\mu\text{A}/\text{cm}^2$ was obtained for the mild steel electrode in 1 M H_2SO_4 solution (Fig. 7). It is observed from the figure that addition of CDHBAP shifts the cathodic and anodic branches toward lower currents, probably as a consequence of the blocking effect of the adsorbed inhibitor molecules. Electrochemical corrosion kinetic data corrosion current density (I_{corr}), corrosion potential (E_{corr}), cathodic and anodic Tafel slopes (b_c , b_a), and inhibition efficiency (IE, %) are given in Table 4.

The efficiency of inhibition (IE, %) was calculated from I_{corr} values by use of the equation:

$$\text{IE } \% = \frac{(I_{\text{corr}(\text{blank})} - I_{\text{corr}(\text{inhibitor})})}{I_{\text{corr}(\text{blank})}} \tag{14}$$

where $I_{\text{corr}(\text{blank})}$ and $I_{\text{corr}(\text{inhibitor})}$ are the corrosion current density without and with inhibitor, respectively. The corrosion current density (i_{corr}) decreases with increasing adsorption of the inhibitor on increasing the inhibitor concentration. A decrease in the corrosion current density with increasing the inhibitor concentration can also be observed from the data presented in Table 4. From the table, it is clear

Table 4 Inhibition efficiency obtained from the cathodic Tafel polarization curve for mild steel in 1 M H_2SO_4 solutions containing different concentrations of CDHBAP at 308 K

Concentration of CDHBAP (ppm)	$-E_{\text{corr}}$ (mV)	i_{corr} ($\mu\text{A}/\text{cm}^2$)	$-b_c$ (mV/decade)	$-b_a$ (mV/decade)	IE (%)
0	565	6,025	205.12	108.01	–
15	517	112.01	157.09	100.04	98.14
25	489	98.30	141.15	73.16	98.36
35	527	63.63	148.23	115.31	98.94
75	523	53.70	155.05	65.28	99.10
100	492	24.36	136.25	65.14	99.59

there is no definite trend in the shift of E_{corr} values in the presence of different concentrations of CDHBAP in 1 M H_2SO_4 . The Tafel slopes (b_a and b_c) are altered in sulfuric acid medium. According to Ferreira et al. [46] and Li et al. [47], if the displacement in corrosion potential is more than 85 mV relative to the corrosion potential of blank solution, inhibitor can be classified as a cathodic or anodic type. The largest shift of E_{corr} is approximately 76 mV in the anodic direction (Table 4). On the basis of these results, CDHBAP is regarded as a mixed-type inhibitor. In other words, addition of CDHBAP to 1 M H_2SO_4 reduces the anodic dissolution of mild steel and also retards the cathodic hydrogen evolution reaction. The cathodic curves give rise to parallel lines, suggesting that addition of CDHBAP to the corrosive environment does not modify the hydrogen evolution reaction and that reduction of H^+ ions at the mild steel surface follows a charge-transfer mechanism. The adsorbed protective film of inhibitor on the mild steel surface impedes corrosion by blocking the reaction sites of the metal. In this way, the actual surface area available for H^+ ions is reduced while the actual reaction mechanism remains unaffected.

AC impedance measurements

The electrochemical behavior of mild steel in inhibited and uninhibited solutions was investigated by electrochemical impedance spectroscopic measurements. Nyquist plots for mild steel in 1 M H_2SO_4 solution in the absence and presence of different concentrations of CDHBAP are shown in Fig. 8.

In this figure, high-frequency (HF) depressed semicircles can be observed. The charge-transfer resistance (R_{ct}) and double-layer capacitance were obtained from the Nyquist plots, and the calculated inhibition efficiency values (IE, %) are reported in Table 5.

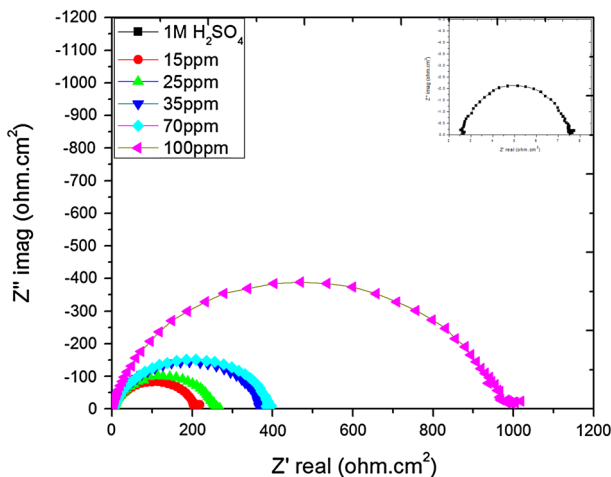


Fig. 8 Nyquist plots for mild steel immersed in 1 M H_2SO_4 (filled squares, inset) and with different concentration of CDHBAP at 308 K

Table 5 Electrochemical impedance data for corrosion of mild steel in 1 M H₂SO₄ solutions containing different concentrations of CDHBAP

Concentration of CDHBAP (ppm)	R_s (Ωcm^2)	R_{ct} (Ωcm^2)	C_{dl} (F/cm ²)	n	IE (%)
0	2.199	3.76	2.94×10^{-2}	0.835	–
15	2.400	210.11	9.07×10^{-6}	0.841	98.20
25	2.024	250.27	6.21×10^{-6}	0.843	98.49
35	2.080	385.94	2.86×10^{-6}	0.862	99.02
75	2.080	396.02	2.66×10^{-6}	0.902	99.05
100	2.200	982.22	4.16×10^{-7}	0.906	99.61

The inhibition efficiencies for each concentration were calculated by use of the formula:

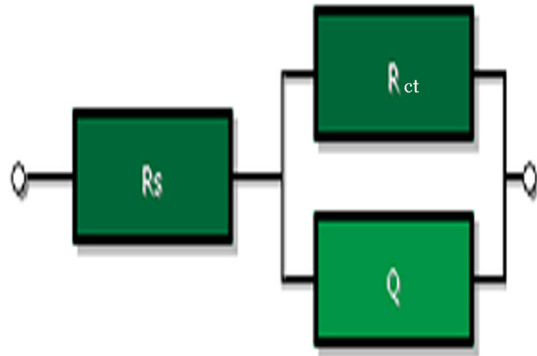
$$\text{IE \%} = \frac{R_{ct(\text{inh})} - R_{ct}}{R_{ct(\text{inh})}} \times 100 \quad (15)$$

where R_{ct} and $R_{ct(\text{inh})}$ are the charge-transfer resistance in the absence and presence of inhibitor, respectively. It is clear from Table 5 that the charge-transfer resistance (R_{ct}) increased from 3.76 to 982.2 Ωcm^2 in the presence of 100 ppm CDHBAP in 1 M H₂SO₄ solution. Values of C_{dl} , however, decrease with an increasing inhibitor concentration. This decrease in C_{dl} is attributed to an increase in the thickness of the electrical double layer. The increase in R_{ct} values is attributed to the formation of an insulating protective film at the metal–solution interface. These observations suggest that CDHBAP functions by adsorption on metal surface, thereby causing a decrease in C_{dl} and an increase in R_{ct} [48]. The change in C_{dl} is caused by gradual replacement of water molecules by the adsorption of inhibitor molecules at the metal–solution interface, which leads to formation of protective film on the mild steel surface which then retards the dissolution reaction. The efficiency of inhibition by the inhibitor increases with increasing inhibitor concentration, because of increased surface coverage. This layer acts as a barrier to mass and charge transfer, retarding dissolution of the metal [49].

EIS spectra were analyzed by use of equivalent circuits (Fig. 9) which represent single charge-transfer reactions. The circuit in Fig. 9 is an example of the classic parallel capacitor and resistor combination. The impedance spectra are described by semicircles in the complex plane to first approximation (Fig. 8). The semicircle is indicative of a charge-transfer process occurring with charge-transfer resistance. A large R_{ct} is associated with a slowly corroding system. The semicircles are observed to be depressed into the Z (real axis) of the Nyquist plot as a result of the roughness of the metal surface. This behavior has been described and discussed by many authors [50–52]. It is modeled by a power-law-dependent capacity term known as the constant phase element (CPE). This kind of phenomenon is known as the “dispersing effect” [53, 54].

Considering that the impedance of a double layer does not behave as an ideal capacitor in the presence of a dispersing effect, a CPE is used as a substitute for the

Fig. 9 The equivalent circuit used to fit the impedance data



capacitor in Fig. 9 to fit the impedance behavior of the electric double layer more accurately. Constant-phase elements have been widely used to account for the deviations caused by surface roughness. The CPE impedance (Z_{CPE}) is obtained as:

$$Z_{\text{CPE}} = \theta^{-1}[(j\omega)^n]^{-1} \quad (16)$$

where ω is the angular frequency ($\omega = 2\pi f$, where f is the ac frequency), with j the imaginary part. Depending upon the value of exponent n , θ may be a resistance, R ($n = 0$), a capacitance, C ($n = 1$), a Warburg impedance, W ($n = 0.5$), or an inductance, L ($n = -1$) [55].

The corresponding fitting results are listed in Table 5 as a function of each concentration.

On the basis of these observations, the equivalent circuit (Fig. 9) was used to fit the experimental impedance data for the different concentrations. The solid curves for all the impedance data obtained by analyzing the corresponding equivalent circuits were close to the experimental data. The value of C_{dl} can be calculated for a parallel circuit composed of a CPE (θ) and a resistor (R_{ct}) by use of the formula:

$$\theta = (R_{\text{ct}} \times C_{\text{dl}})^n / R_{\text{ct}} \quad (17)$$

The efficiency of inhibition by CDHBAP was evaluated from the R_{ct} values of the impedance. The more densely packed the monolayer of the inhibitor, the larger the diameter of the semicircle, which results in higher R_{ct} and lower C_{dl} . According to the fitting results (Table 5), R_{ct} increases with increasing inhibitor concentration whereas C_{dl} tends to decrease. A large value of R_{ct} is associated less corrosion. Furthermore, better protection provided by an inhibitor is associated with a decrease in C_{dl} . The increasing value of n with increasing inhibitor concentration could be explained on the basis of a reduction in surface heterogeneity, because of adsorption of the inhibitor on the most active adsorption sites [56].

FT-IR study

FT-IR studies are conducted to determine the functional groups present in organic compounds and the type of bonding of organic inhibitors to the metal surface [57].

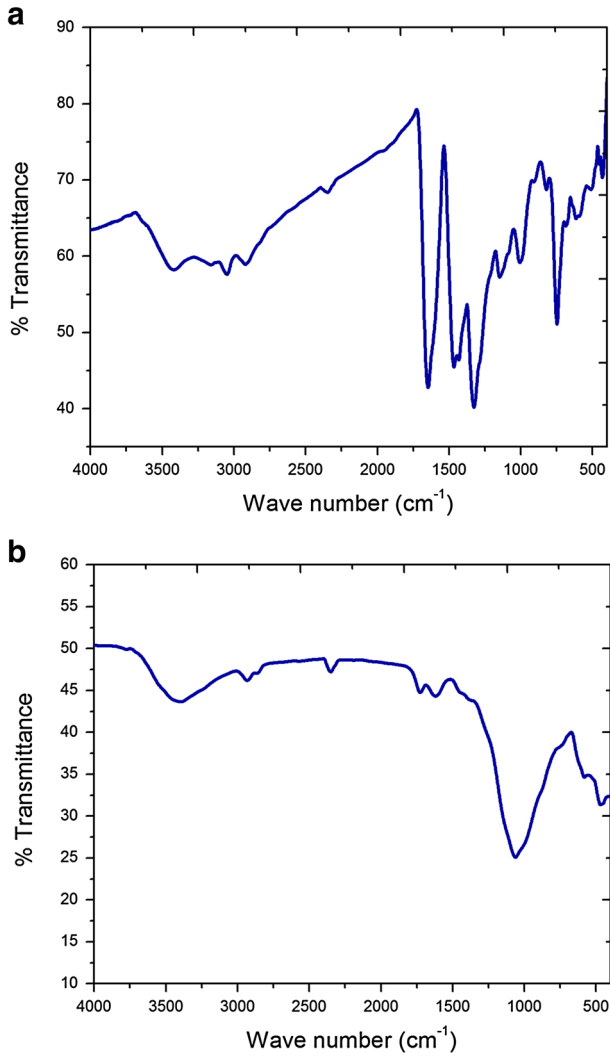


Fig. 10 FT-IR spectra of (a) CDHBAP (b) surface film of the mild steel specimen immersed in 1 M H_2SO_4 + CDHBAP

The FT-IR spectrum of pure CDHBAP is shown in Fig. 10a. Original absorption at 3419 cm^{-1} is overlapped by the strong stretching mode of N–H. The sharp peaks at $1,647\text{ cm}^{-1}$ are attributed to C=O stretching vibrations and the peaks at $3,047\text{ cm}^{-1}$ are related to C–H stretching vibrations of the aromatic ring. Bands at $1,147$ and $1,327\text{ cm}^{-1}$ arise from C–N stretching of the aromatic ring. The peak at $1,461\text{ cm}^{-1}$ corresponds to the N–H bending vibration of the amide group [58]. The peak at 748 cm^{-1} is the C–H bending vibration of benzene.

The Fourier-transform infrared spectrum of the adsorbed protective layer formed on the mild steel surface after immersion in 1 M H_2SO_4 containing CDHBAP is

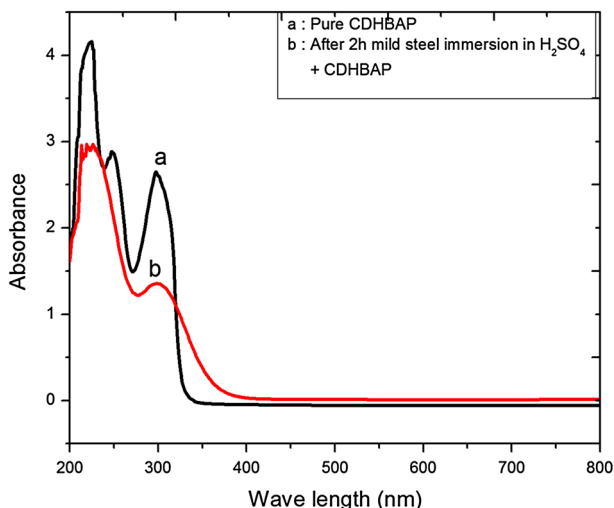
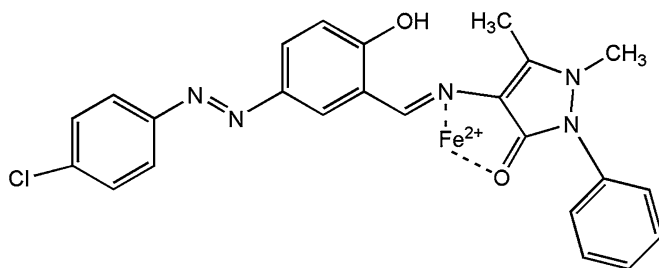


Fig. 11 (a) UV spectrum of pure CDHBAP. (b) Spectrum after immersion of mild steel in 1 M H_2SO_4 + 100 ppm CDHBAP for 2 h at 308 K

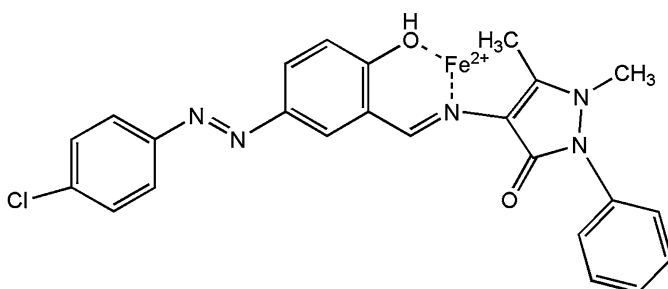
shown in Fig. 10b. Comparison of Fig. 10a, b reveals that all the important peaks in the pure compound are present in the adsorption layer on the steel surface. The band at approximately $1,620\text{ cm}^{-1}$ is attributed to C=O stretching vibrations. The appearance of this peak in the adsorbed layer indicates that the oxygen atom and the carbonyl group did not contribute to the adsorption process. The broad band at $3,398\text{ cm}^{-1}$ is attributed to O–H stretching, which indicates that the protective film contains H_2O . N–H stretching vibrations are absent from the FT-IR spectrum of the adsorbed protective layer, revealing that nitrogen and oxygen atoms are acting as active centers in adsorption. Overall study of the results suggests that inhibitors are adsorbed on the mild steel surface.

UV–visible spectroscopic investigation

Measurement of the absorption of monochromatic light enables quantitative analysis of metal complexes, because adsorption is proportional to the concentration of the absorbing species [59]. UV–visible absorption is a sensitive direct method for spectrometric detection. The electronic absorption spectrum of CDHBAP contains three bands in UV region as shown in Fig. 11a. The shorter wavelength peaks with λ_{max} at 225, 247, and 297 nm are ascribed to π – π^* and n – π^* transitions of the carbonyl group and heterocyclic ring present in the inhibitor. After immersion for 2 h (Fig. 11b) the band at 247 nm completely disappears, and the change in the position of absorption maximum (or change in absorbance) is indicative of the formation of a complex between two species in solution. However, there is no significant change in the shape of the spectra [60, 61]. CDHBAP can react with the Fe^{2+} ion by two routes, giving structures I and II (Fig. 12). Therefore, formation of two different complexes is possible. In complex II, the six-membered ring is stable;



Structure I



Structure II

Fig. 12 CDHBAP complexes

in complex I, however, the five membered rings formed are most stable for chelates containing single or double bonds. Thus structure I is preferable.

XRD studies

X-ray diffraction was used to study film formation on mild steel in different test solutions. The XRD patterns are presented in Fig. 13. The patterns obtained clearly reveal the presence of metal and metal oxide phases [62]. When the diffraction data for several oxides and oxy hydroxides of iron were analyzed, iron peaks appears at $2\theta = 45.4^\circ, 82.9^\circ, 99^\circ$ and the peaks at $2\theta = 35.5^\circ, 42.9^\circ, 64.9^\circ$ can be assigned to oxides of iron. It is observed that the surface of the metal immersed in 1 M H_2SO_4 alone contains Fe_3O_4 and $FeOOH$. In the presence of CDHBAP, however, peaks arising from oxides of iron, for example Fe_3O_4 and $FeOOH$, are absent and the iron peaks at $2\theta = 45.4^\circ, 82.9^\circ, 99^\circ$ are very intense. This is indicative of formation of an adsorbed protective film on the surface of the metal in the presence of CDHBAP. The results clearly prove the effect of CDHBAP on corrosion of mild steel in acid.

SEM studies

SEM micrographs, with appropriate magnification, are depicted in Fig. 14. Figure 14a shows the finely polished surface of mild steel and the small scratches

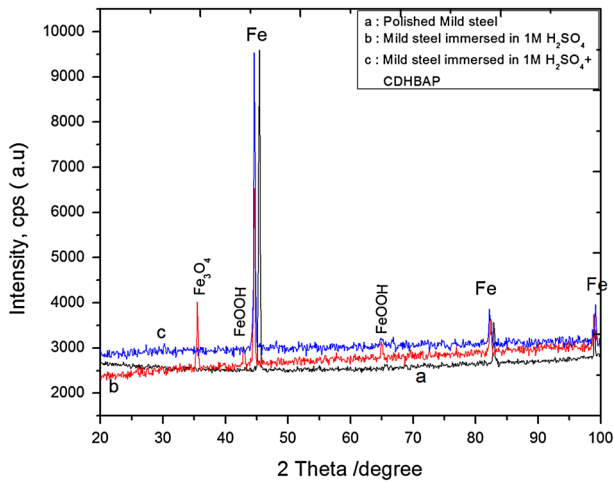


Fig. 13 XRD patterns of (a) polished mild steel (b) mild steel after immersion in 1 M H₂SO₄ (c) mild steel after immersion in 1 M H₂SO₄ in the presence of CDHBAP

which arose during abrasion. The morphology of the specimen surface in Fig. 14b revealed that the specimen was highly damaged in the presence of 1 M H₂SO₄ solutions, because of direct attack by the aggressive acid. Figure 14c shows the appearance of smooth mild steel surfaces after addition of CDHBAP to the 1 M H₂SO₄ solutions. It can be seen from Fig. 14c that the rate of corrosion is reduced and the smooth surface is preserved by formation of a protective film on the metal surface, which is responsible for inhibition of corrosion.

Mechanism of inhibition

It is well recognized that organic inhibitor molecules are adsorbed on the metal surface. The adsorption process is affected by the chemical structure of the inhibitors, the nature and charged surface of the metal, and the distribution of charge over the whole inhibitor molecule. In general, owing to the complex nature of adsorption and the inhibitive action of the inhibitor, single modes of adsorption of the inhibitor on the metal surface are not possible. Organic inhibitor molecules may be adsorbed by the metal surface by one or more of the following mechanisms:

- 1 electrostatic interaction between the charged molecules and the charged metal;
- 2 interaction of unshared electron pairs in the molecule with the metal;
- 3 interaction of π -electrons with the metal; and/or
- 4 a combination of these [63, 64].

The efficiency of inhibition depends on many factors, including molecular size, heat of hydrogenation, mode of interaction, with the metal surface, formation of metallic complexes, and the charge density on the adsorption sites [65]. The efficiency of inhibition by CDHBAP may be attributed to the presence of electron-

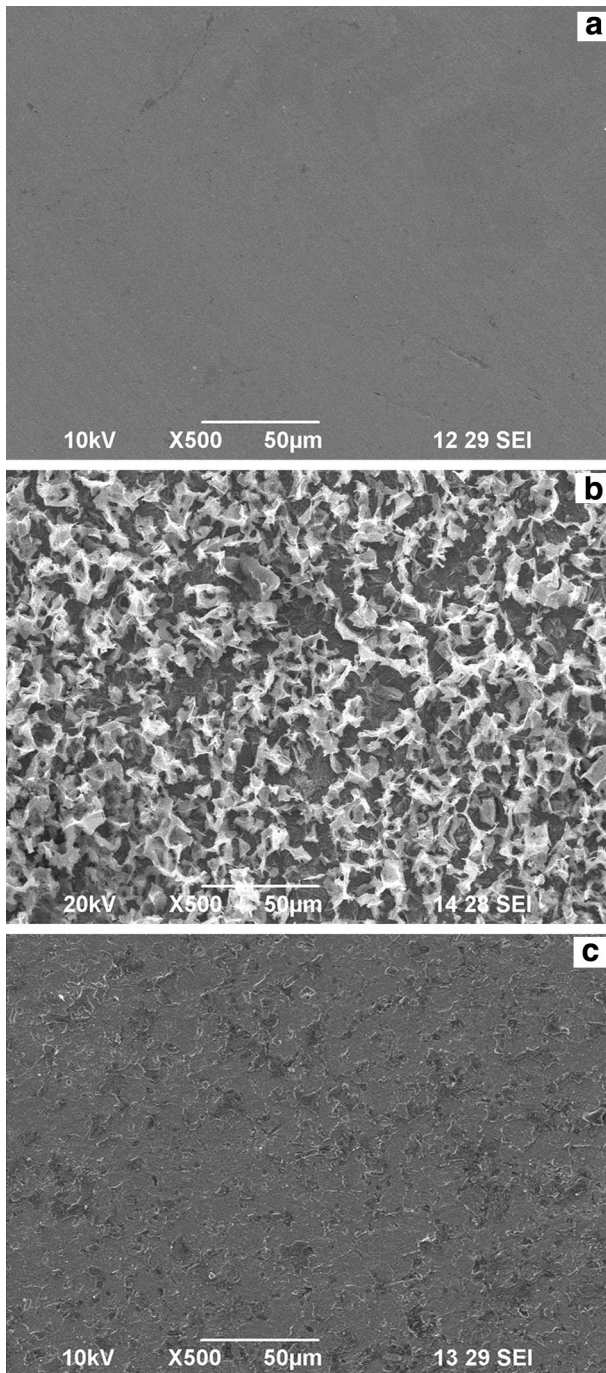
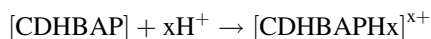


Fig. 14 SEM images of mild steel surfaces **a** polished mild steel **b** mild steel after immersion in 1 M H₂SO₄ **c** mild steel after immersion in 1 M H₂SO₄ + 100 ppm CDHBAP

rich N and O atoms and the aromatic ring. A phenyl ring, a hydroxyl group, an amide linkage, and two electron-donating methyl groups are present in the structure of CDHBAP. Therefore, possible reaction centers are the unshared electron pair of heteroatoms and π -electrons of the aromatic ring. From the experimental and theoretical results obtained, the adsorption and inhibition effect of CDHBAP in 1 M H_2SO_4 solution can be explained as follows. Schiff bases may be protonated in the acid solution as:



In aqueous acidic solutions, CDHBAP is present either as the neutral molecule or as protonated CDHBAP (cation). Two modes of adsorption by the surface of the metal can be considered. In one mode, neutral CDHBAP is adsorbed on the surface of the mild steel by chemisorption involving displacement of water molecules from the metal surface and sharing of electrons between heteroatoms such as nitrogen and oxygen and the metal surface. The inhibitor molecules can also be adsorbed by the mild steel surface on the basis of donor–acceptor interactions between p-orbitals of the heterocyclic ring and vacant d-orbitals on the iron surface. In another mode, because it is well known that the steel surface is positively charged in acid solution [66], it is difficult for the protonated CDHBAP to approach the positively charged mild steel surface (H_3O^+ –metal interface) because of electrostatic repulsion. The protonated CDHBAP is adsorbed as a result of electrostatic interactions between the positively charged molecules and the negatively charged metal surface. It should be noted that the molecular structure of protonated CDHBAP is unchanged relative to the neutral form, the N-atoms on the ring remaining strongly blocked. So when protonated CDHBAP is adsorbed by the metal surface, coordinate bonds may be formed by partial transfer of electrons from the hetero atoms to the metal surface.

Conclusions

The following main conclusions are drawn from this study. The efficiency of inhibition by this inhibitor increases with increasing inhibitor concentration but decreases with increasing temperature. Polarization curves prove that CDHBAP is a mixed-type inhibitor. AC impedance plots indicate that charge-transfer resistance increases and double layer capacitance decreases with addition of inhibitor. CDHBAP is adsorbed by the mild steel surface in accordance with the Langmuir adsorption isotherm; the negative value of the Gibbs free energy of adsorption (ΔG_{ads}^0) is indicative of a strong interaction between the inhibitor molecules and the mild steel surface. FT-IR, XRD, and SEM results confirm the formation of a protective surface layer on the mild steel surface. UV–visible studies clearly reveal the formation of a the complex responsible for inhibition of corrosion. Weight loss, polarization, and electrochemical impedance spectroscopy measurements are in good agreement.

References

1. M. Anwar Sathiq, A.J. Abdul Nasser, P.M. Sirajudeen, *Eur. J. Chem.* **8**, 621 (2011)
2. M. Lagrenee, B. Mernari, N. Chaibi, M. Traisnel, H. Vezin, F. Bentiss, *Corros. Sci.* **43**, 951 (2001)
3. A.J. Abdul Nasser, M. Anwar Sathiq, *Arabian J. Chem.* (2011). doi:[10.1016/j.arabjc.2011.07.024](https://doi.org/10.1016/j.arabjc.2011.07.024)
4. M.R. Singh, K. Bhrara, G. Singh, *Port. Electrochim. Acta.* **26**, 479 (2008)
5. M. Bouklah, A. Attayibat, S. Kertit, A. Ramdani, B. Hammouti, *Appl. Surf. Sci.* **242**, 399 (2005)
6. M. Ajmal, A.S. Mideen, M.A. Quraishi, *Corros. Sci.* **36**, 79 (1994)
7. B.I. Ita, O.E. Offiong, *Mater. Chem. Phys.* **48**, 164 (1997)
8. B. Mernari, H.A. Attari, M. Traisnel, F. Bentiss, M. Lagrenee, *Corros. Sci.* **40**, 391 (1998)
9. R.T. Morrison, R.N. Boyd, *Organic Chemistry*, IV edn. (Universal Book Stall, New Delhi, 1983), pp. 1277–1284
10. P. Xuehui, H. Baorong, L. Weihua, L. Faqian, Y.U. Zhigang, *Chin. J. Chem. Eng.* **15**, 909 (2007)
11. S.S. Abdul-Rehim, K.F. Khaled, N.A. Mobarak, *Arabian J. Chem.* **4**, 333 (2011)
12. F. Bentiss, M. Lagrenee, M. Traisnel, J.C. Hornez, *Corros. Sci.* **41**, 789 (1999)
13. M. Lagrenee, B. Mernari, M. Bouanis, M. Traisnel, F. Bentiss, *Corros. Sci.* **44**, 573 (2002)
14. V.V. Dhayabaran, I.S. Lydia, J.P. Merlin, P. Srenganayaki, *Ionics* **10**, 123 (2004)
15. M.M. Mennucci, E.P. Banczek, P.R.P. Rodrigues, I. Costa, *Cem. Concr. Compos.* **31**, 418 (2009)
16. A. Popova, E. Sokolova, S. Raicheva, M. Christov, *Corros. Sci.* **45**, 33 (2003)
17. K.F. Khaled, M.A. Amin, *Corros. Sci.* **51**, 1964 (2009)
18. K. Tebbji, H. Oudda, B. Hammouti, M. Benkaddour, M.E. Kodadi, F. Malek, M. Ramdani, *Appl. Surf. Sci.* **241**, 326 (2005)
19. K. Laarej, M. Bouachrine, S. Radi, S. Kertit, B. Hammouti, *Eur. J. Chem.* **7**, 419 (2010)
20. F. Touhami, B. Hammouti, A. Aouniti, S. Kertit, *Ann. Chim. Sci. Mater.* **24**, 581 (1999)
21. M. Abdallah, M.M. El-Naggar, *Mater. Chem. Phys.* **71**, 291 (2001)
22. K.F. Khaled, S.S. Abdul-Rehim, G.B. Sakr, *Arabian J. Chem.* **5**, 213 (2012)
23. L. Herrag, A. Chetouani, S. Elkadiri, B. Hammouti, A. Aouniti, *Port. Electrochim. Acta.* **26**, 211 (2008)
24. K. Tebbji, I. Bouabdellah, A. Aouniti, B. Hammouti, H. Oudda, M. Benkaddour, M. Ramdani, *Mater. Lett.* **61**, 799 (2007)
25. C. Anitha, C.D. Sheela, P. Tharmaraj, S. Sumathi, *Spectrochim. Acta Mol. Biomol. Spectrosc.* **96**, 493 (2012)
26. T. Ibrahim, M. Habbab, *Int. J. Electrochem. Sci.* **6**, 5357 (2011)
27. X. Li, S. Deng, H. Fu, *Corros. Sci.* **62**, 163 (2012)
28. D.K. Yadav, M. Quraishi, *Ind. Eng. Chem. Res.* **51**, 14966 (2012)
29. M.G. Sethuraman, V. Aishwarya, C. Kamal, T. Jebakumar Immanuel Edison, *Arabian J. Chem.* (2013). doi:[10.1016/j.arabjc.2012.10.013](https://doi.org/10.1016/j.arabjc.2012.10.013)
30. R. Karthikaiselvi, S. Subhashini, *Arabian J. Chem.* (2012). doi:[10.1016/j.arabjc.2012.10.024](https://doi.org/10.1016/j.arabjc.2012.10.024)
31. M. Sobhi, M. Abdallah, K.S. Khairou, *Monatsh. Chem.* **143**, 1379 (2011)
32. A.R.S. Priya, V.S. Muralidharam, A. Subramania, *Corrosion* **64**, 541 (2008)
33. A.K. Singh, M.A. Quraishi, E.E. Ebenso, *Int. J. Electrochem. Sci.* **6**, 5676 (2011)
34. M.A. Quraishi, A. Singh, V.K. Singh, D.K. Yadav, A.K. Singh, *Mater. Chem. Phys.* **122**, 114 (2010)
35. H. Cang, W. Shi, J. Shao, Q. Xu, *Int. J. Electrochem. Sci.* **7**, 3726 (2012)
36. A. Singh, I. Ahamad, V.K. Singh, M.A. Quraishi, *J. Solid State Electrochem.* **15**, 1087 (2011)
37. A.K. Singh, S. Khan, A. Singh, S.M. Quraishi, M.A. Quraishi, E.E. Ebenso, *Res. Chem. Intermed.* **39**, 1191 (2013)
38. Z. Szklarska-Smialowska, J. Mankowski, *Corros. Sci.* **18**, 953 (1978)
39. A. Yurt, S. Ulutas, H. Dal, *Appl. Surf. Sci.* **253**, 919 (2006)
40. X. Li, S. Deng, H. Fu, *Prog. Org. Coat.* **67**, 420 (2010)
41. D.A. Jones, *Principles and Prevention of Corrosion* (Macmillan, New York, 1992)
42. N.V. Likhanova, M.A. Dominguez-Aguilar, O. Olivares-Xometi, N. Nava-Entzana, E. Arce, H. Dorantes, *Corros. Sci.* **52**, 2088 (2010)
43. H.J. Flitt, D. Paul Schweinsberg, *Corros. Sci.* **47**, 3034 (2005)
44. B. Rosborg, J. Pan, C. Leygraf, *Corros. Sci.* **47**, 3267 (2005)
45. E. McCafferty, *Corros. Sci.* **47**, 3202 (2005)
46. E.S. Ferreira, C. Giancomelli, F.C. Giacomelli, A. Spinelli, *Mater. Chem. Phys.* **83**, 129 (2004)
47. W.H. Li, Q. He, C.L. Pei, B.R. Hou, *J. Appl. Electrochem.* **38**, 289 (2008)

48. I. Naqvi, A.R. Saleemi, S. Naveed, *Int. J. Electrochem. Sci.* **6**, 146 (2011)
49. G. Avci, *Colloid Surf. A* **317**, 730 (2008)
50. W. Schelder, *J. Phys. Chem* **79**, 127 (1975)
51. T. Pojkassy, *J. Electroanal. Chem.* **364**, 111 (1994)
52. W.R. Fawcett, Z. Kovacova, A. Motheo, C. Foss, *J. Electroanal. Chem.* **326**, 91 (1992)
53. F. Mansfeld, *Corrosion* **37**, 301 (1981)
54. E. Maccafferty, *Corros. Sci.* **39**, 243 (1997)
55. B.A. Boukamp, *Solid State Ionics* **20**, 929 (1986)
56. A. Popova, M. Chirstov, *Corros. Sci.* **48**, 3208 (2005)
57. L. Li, X. Zhang, J. Lei, J. He, S. Zhang, F. Pan, *Corros. Sci.* **63**, 82 (2012)
58. R.A. Ahmed, R.A. Farghali, A.M. Fekry, *Int. J. Electrochem. Sci.* **7**, 7270 (2012)
59. M. Gopiraman, C. Sathya, S. Vivekananthan, D. Kesavan, N. Sulochana, *J. Mater. Eng. Perform.* **16**, 240 (2012)
60. I.B. Obot, N.O. Obi-Egbedi, A.O. Eseola, *Ind. Eng. Chem. Res.* **50**, 2098 (2011)
61. A. Singh, M.A. Quraishi, E.E. Ebenso, *Int. J. Electrochem. Sci.* **7**, 12545 (2012)
62. D. Gopi, K.M. Govindaraju, V.C.A. Prakash, V. Manivannan, L. Kavitha, *J. Appl. Electrochem.* **39**, 269 (2009)
63. D.P. Schweinsberg, G.A. George, A.K. Nanayakkara, D.A. Steiner, *Corros. Sci.* **28**, 33 (1988)
64. H. Shorky, M. Yuasa, I. Sekine, R.M. Issa, H.Y. El-Baradie, G.K. Gomma, *Corros. Sci.* **40**, 2173 (1998)
65. Y. Abbouda, A. Abourriche, T. Saffaj, M. Berrada, M. Charrouf, A. Bennamara, N. Al Himidi, H. Hannache, *Mater. Chem. Phys.* **105**, 1 (2007)
66. G.N. Mu, T.P. Zhao, M. Liu, T. Gu, *Corrosion* **52**, 853 (1996)